6 CHAPTER

AN OPTIMIZED MULTI-STABLE STOCHASTIC RESONANCE FOR THE ENHANCEMENT OF PITUITARY MICROADENOMA IN MRI

Highlights of the Chapter

- *The present chapter proposes an algorithm for enhanced visualization of microadenoma in pietuitary gland*
- *The algorithm for enhancement of MRI data is based on multi-stable stochastic resonance (MSSR) technique*
- *The dynamic parameters of MSSR are optimized using multi-objective ant lion optimization*
- *More area between the mean intensity vs. phase curve for processed set of images shows more confidence level of in the diagnosis*

Abstract

Magnetic resonance imaging (MRI) is the modality of choice as far as imaging diagnosis of pathologies in the pituitary gland is concerned. Further, the advent of dynamic contrast enhanced (DCE) has enhanced the capability of this modality in detecting minute benign but endocrinologically significant tumors called microadenoma. These lesions are visible with difficulty and a low confidence level in routine MRI sequences, even after administration of

intravenous gadolinium. Techniques to enhance the visualization of such foci would be an asset in improving the overall accuracy of DCE-MRI for detection of pituitary microadenomas. The present study proposes an algorithm for post-processing DCE-MRI data using multi-stable stochastic resonance (MSSR) technique. Multi-objective ant lion optimization (MOALO) optimizes the contrast enhancement factor (CEF) and anisotropy of an image by varying the parameters associated with the dynamics of MSSR. The marked regions of interest (ROIs) are labeled as normal and microadenoma of pituitary obtained with increased level of accuracy and confidence using proposed algorithm. The increased difference between the mean intensity curves obtained using these ROIs validated the obtained subjective results. Further, the proposed MSSR based algorithm has been evaluated on standard T1 and T2 weighted BrainWeb dataset images and quantified in terms of CEF, peak signal to noise ratio (PSNR), structure similarity index measure (SSIM) and universal quality index (UQI). The obtained mean values of CEF as 1.22, PSNR as 27.68, SSIM as 0.75, and UQI as 0.83 for twenty dataset images. These values are highest for proposed method among considered existing contrast enhancement algorithms.

6.1 Introduction

The pituitary gland is an endocrine organ of prime importance as it produced a number of vasoactive bio-metabolites (known as hormones) which control most of the endocrine functions in human body. Pathologies in this gland can alter the human physiology either by increasing or by impeding the production of these hormones. Pituitary adenomas are usually benign tumors, which are conventionally classified as being a microadenomas or a macroadenomas depending on a cut-off size of 1 cm. A macroadenoma can be easily visualized of routine MRI sequences by virtue of large size and typical signal intensity

pattern. On the other hand, a microadenoma is mostly suspected during investigation of an altered hormonal milieu in human system. Direct visualization of microadenomas has always been a challenge for medical imaging and remains of prime importance as these lesions can be surgically enucleated resulting in cure [191]. Ultrafast T1W MRI sequences with intravenous gadolinium, thin slices and a small field of view coned down to sella have now been made possible by heavy-duty gradient coils and advanced gradient recalled echo (GRE) sequences, labelled as dynamic contrast enhanced (DCE) MRI. The technique enables plotting of the signal enhancement caused due to the passage of intravenous gadolinium as a function of time, and subsequently using the arterial input function to generate perfusion maps. Subsequently, region of interest (ROI) analysis of various suspicious spots with internal validation to normal regions can help detection of microadenoma. The philosophy is to take advantage of the fact that most microadenomas enhance subsequent to normal pituitary parenchyma due to their typical pattern of blood flow. Occasionally however, DCE-MRI renders certain false negative and false positive results due to inherent areas of variable contrast enhancement [192]. Tissue specific post-processing of DCE-MRI data may be useful for better analysis of microadenoma in pituitary and can be achieved by accurate image processing operations: (i) de-noising and (ii) post-processing contrast enhancement.

The research challenge of medical image enhancement is optimum contrast enhancement along with low noise as both together have an important guarantee of better image quality. Previously proposed techniques such as linear minimum mean square estimation [193], wavelet transformation [194, 195] and non-local means algorithms principle component analysis [25] successfully de-noised the MRI data. However, there is no improvement in the contrast using those techniques, hence, could not enhanced the information where two

different tissues have low pixel differences. On the other hand maximum likelihood gamma distribution technique based on histogram modification [196] and multi-scale morphological approach based method [50] worked well for contrast enhancement with better peak signal to noise ratio (PSNR) in comparison to conventional histogram equalization (HE) and contrast limited adaptive histogram equalization (CLAHE) methods. However, images produced by these techniques are non-optimum in terms of contrast and PSNR. The tradeoff between image contrast and noise suggest that there is requirement of an algorithm that can produce maximum contrast at the cost of lowest noise. The objective of this work is to improve the contrast by keeping least noise in optimum manner for low contrast noisy MRI data.

Dynamic stochastic resonance (DSR) uses the noise as a free source of energy and found useful to enhance the information [147, 197]. In presence of a nonlinear dynamic system, DSR reduces the noise and enhances the weak signal. In comparison to conventional enhancement methods, stochastic resonance (SR) uses the noise contains in the image to increase the contrast between the tissues. This technique also found useful in better image segmentation of pathological liver CT images and left ventricle [198].

DSR based methods has been proposed for the enhancement of ultrasound images [109] and MR images [54]. In these methods, the enhancement effects of image features obtained by adjustment of the system parameters manually or non-optimum manner. Recently, a good advancement over the previously proposed DSR based method has been seen where, the model structure is automatically adjusted using particle swarm optimization (PSO) [136]. This study selected DSR parameters for the objective of enhancement of low contrast diffusion weighted MRI data. Implementation of modified bi-stable resonance neuron model was also a good effort to obtained better enhancement of MRI data [199]. These approaches

find near optimum image quality; however, quartic bi-stable resonance model limits the post-processing enhancement of small pituitary in DCE MRI data. For effective extraction of the information from low tissue contrast noisy image, the classical DSR methods need to be replaced with an improved resonance model. Hence, the present study introduces the efficient algorithm based on MOALO optimized MSSR for the enhancement of DCE MRI data. Recently, MSSR also studied for the weak signal detection for mechanical fault detection of rolling bearing and performed better than classical DSR, however, J. Li et al. have not attempted for optimized MSSR parameters [106].

In present work, wavelet based MSSR has been used to enhance the MRI data and found useful in the diagnosis of microadenomas in pituitary gland. The MOALO [200] tunes the MSSR parameters for the maximization of CEF and anisotropy of an image, which enables proposed algorithm to pick and enhance the useful clinical evidences. Section 6.2 presents the brief introduction, theory and characteristics of MSSR. This section also describes the mono-stable, bi-stable and tri-stable resonance models from a common MSSR model. Section 6.3 discusses the MOALO algorithm, formulates the objective and constraints. Section 6.4 discussed the material and methods used for the study. Section 6.5 analyzes the performance of MSSR on simulated T1 weighted and T2 weighted MRI dataset. The tri-stable resonance model found better than the bi-stable resonance model in terms of image contrast and anisotropy. Second part of this section shows the image enhancement capability of MSSR method on real dynamic contrast based MRI data for pituitary enhancement and found helpful in the diagnosis of microadenomas. This section also compares the classical quartic bi-sable technique with proposed MSSR algorithm. Finally, section 6.6 concluded the whole study.

6.2 Wavelet based Multi-Stable Stochastic Resonance

MSSR can have three resonance models (i) mono-stable, (ii) bi-stable and (iii) tri-stable depending on the associated DSR parameters as shown in Fig. 6.1. A Brownian particle needs to cross two potential barriers once a half cycle to match the frequency of input signal for the resonance in the case of tri-stable model as it has two barrier and three potential wells. On the other hand, the same particle needs to cross only one potential barrier in case of bi-stable model. For a cycle, the tri-stable model has a greater moving distance of the Brownian particle in comparison to bi-stable model. Hence, tri-stable requires more energy to match the transition rate of the particle with the frequency of input signal. Once, the system gets the required energy in the form of the intensity of noise, the resonance occurs and the signal get enhanced. In short, structural characteristics of tri-stable model leads to its better performance in comparison to the mono-stable and bi-stable model. The efficiency of a resonance model has been presented in terms of work done by periodic force [16] and SNR [18] with respect to parameters associated with the model. The tri-stable system has the capability to works with low contrast and noisy images better than the bi-stable system. The transition of a Brownian particle between the states having multi-stable potential given by as follows [16]:

$$U(x) = \frac{x^6}{6a} - \frac{(1+c)x^4}{4b} + \frac{cx^2}{2} \qquad (6.1)$$

where a, b are the model parameters with positive real values, c model parameter with real values and x is the particle's position axis centered on the origin $x = 0$. Motion of particle is derived using the algebraic sum of derivative of multi-stable potential, week periodic input signal $s(t)$ and noise input $\eta(t)$ to the system. Hence:

$$\frac{dx}{dt} = -\frac{x^5}{a} + \frac{(1+c)x^3}{b} - cx + s(t) + \eta(t) \quad (6.2)$$

This study uses the internal noise of the image, hence $s(t) + \eta(t)$ is considered as the discrete wavelet transformation (DWT) of the image $I(i,j)$. The DWT of image $I(i,j)$ having $M \times N$ size defines as follows:

$$W(l_0,p,q) = \frac{1}{\sqrt{MN}} \sum_{i=1}^{M} \sum_{j=1}^{N} I(i,j) \phi_{l_0,p,q}(i,j) \quad (6.3)$$

$$W_{\Psi}^{s}(l,p,q) = \frac{1}{\sqrt{MN}} \sum_{i=1}^{M} \sum_{j=1}^{N} I(i,j) \Psi_{l,p,q}^{s}(i,j) \quad (6.4)$$

where $W(l_0,p,q)$ define as the approximation coefficients of I at scale l_0, whereas $W_{\Psi}^{s}(l,p,q)$ add horizontal, vertical and diagonal details for $l \geq l_0$, s belongs to any of (H,V,D) and l_0 is an arbitrary starting scale. The filter transforms the original spatial distribution of intensities into a spatial distribution of correlations that has the visual appearance of the original image but with the strong highlighting of the regions whose size is similar to the wavelet size. The approximation coefficients have low-pass information of the image, hence enhancement of these coefficients are less susceptible to noise. In context with the current approach, these coefficients undergo MSSR. Rewrite Equation (6.2) as:

$$\frac{dx}{dt} = -\frac{x^5}{a} + \frac{(1+c)x^3}{b} - cx + input \quad (6.5)$$

where $input$ is approximation coefficients, cA of wavelet transformed image. Equation (6.5) discretizes in k steps using Euler-Maruyama's method [201] to process approximation coefficients that are discreet in nature:

$$x(n+1) = x(n) + \left[-\frac{x(n)^5}{a} + \frac{(1+c)x(n)^3}{b} - c\,x(n) + cA\right] \quad (6.6)$$

The dynamic equation shown in Equation (6.6) may leads to three explicit models depending on the parameter combination of a, b and c. Li et al. [106] calculated the parameters distribution of multi-stable system for the detection of week signal; however, these values are not suitable for the image enhancement applications. The potential function $U(x)$ acts as a bi-stable system for all the values of 'c' less than zero, whereas this function will act as either tri-stable or mono-stable state for all positive values of 'c'. Experimentally, we observed that the $U(x)$ turns to mono-stable for $b > 1.2 \times 10^5$ and tri-stable for $b < 1.2 \times 10^5$, if $c \geq 0$ and $10^{10} < a < 10^{11}$. This range of values is useful for the image enhancement of different MRI sequences.

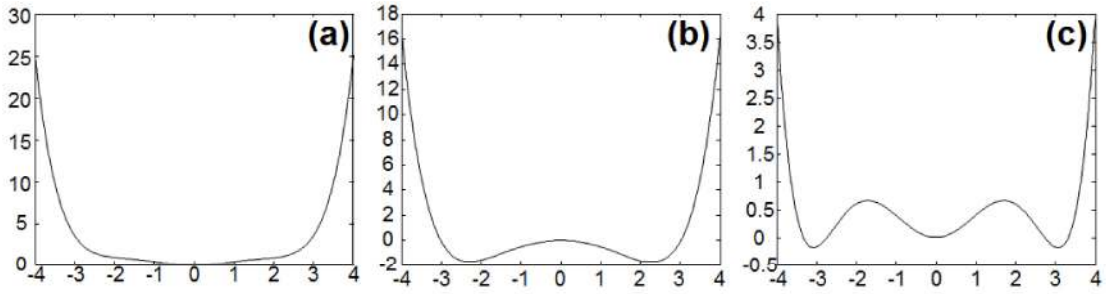

Figure 6-1: Multi-stable potential function in (a) mono-stable state corresponding to a=15, b=4.5, c=1, (b) bi-stable state corresponding to a=28, b=4.5, c=-1, and (c) tri-stable state corresponding to a=28, b=4.5, c=1

6.3 Multi-objective Ant lion optimization

Ant lion optimization (ALO) is an evolutionary computation technique, motivated by the unique hunting behavior of antlions in the hunting of their favorite prey i.e. ants. Every ant moves randomly in nature during the searching for prey. Random walks of ants need to be normalized to prevent the ants from overshooting as follows [98]:

$$X_j^t = \frac{(X_j^t - min_j) \times (d_j^t - c_j^t)}{max_j - min_j} + c_j^t \qquad (6.7)$$

$where\ min_j$ and max_j are the minimum and maximum of random walk in j^{th} variable respectively, c_j^t and d_j^t indicates the minimum and maximum of j^{th} variable at t^{th} iteration respectively. ALO algorithm defines the new minimum and the new maximum of each variables in every iteration by adding minimum and maximum of a variable to the position of the antlion. Hence, affect the random walks of ants as follow:

$$c_j^t = AL_i^t + c^t \tag{6.8}$$

$$d_j^t = AL_i^t + d^t \tag{6.9}$$

$where\ c^t$ and $d^t$are the minimum and maximum of all variables at t^{th} iteration respectively and AL_i^t shows the position of i^{th} antlion at t^{th} iteration. Further, these minimum and maximum values of variable decrease adaptively in following manner: $c^t = \frac{c^t}{R}$, $d^t = \frac{d^t}{R}$, and hence, the range variable moves toward the position of the antlion. In this study, the MSSR parameters a, b, c act as the variables for MOALO.

The ratio $R = 10^w \frac{t}{T}$, $where\ w$ is a constant, helps to regulate the accuracy level of exploitation, t is the current iteration and T is the maximum number of iterations. As the ant reaches the bottom of the pit, it is caught by antlion. Further, an antlion updates its position to improve its chances of catching new ant in the following manner:

$$AL_i^t = Ant_j^t \text{ if } f\left(Ant_j^t\right) \prec f\left(AL_i^t\right) \tag{6.10}$$

$where\ t$ shows current iteration and Ant_j^t shows the position of j^{th} ant at t^{th} iteration. The fittest antlion is called elite and it affects the movement of all the ants during iterations. Hence, the position of an ant, as follows:

$$Ant_j^t = \frac{R_A^t + R_E^t}{2} \quad (6.11)$$

$where\ R_A^t$ is ant's random walk around particular antlion and R_E^t is ant's random walk around the elite antlion.

MOALO uses niching approach for the distribution of the solution in the archive [200], where the neighborhood of every solution is explored in a pre-defined radius. The MOALO algorithm selects antlions from the solutions those have the minimum populated neighborhood. The probability of selecting a solution set from the archive is: $P_j = \frac{k}{N_j}$, $where\ k > 1$ and N_j is the number of solutions in the neighborhood of j^{th} solution. When the archive is fully occupied, the solutions having most populated neighborhood are replaced with new solutions. The probability of removing the solution is: $P_j = \frac{N_j}{k}$. MOALO uses the roulette wheel and (11) to select a non-dominated solution from the archive.

ALO provides superior results in terms of exploration and exploitation [98]. Good exploration ensures that the potential areas of the search space are properly explored and prevent the algorithm to trap in local optima, which is guaranteed by the random walks of ants nearby the antlion and the random selection of the antlions. On the other hand, the shrinking boundaries of the trap ensure good exploitation.

6.3.1 Problem objectives

6.3.1.1 Maximization of contrast enhancement factor

Descriptor for an image quality Q defined as the ratio of variance (σ^2) and mean (μ) of the pixel intensity of image [54]:

$$Q = \frac{\sigma^2}{\mu} \quad (6.12)$$

$where\ \sigma$ is standard deviation and μ is the mean of the image. The value of contrast enhancement factor (CEF) obtained by calculating the ratio of post enhancement value of image quality index Q_B and pre enhancement value of image quality index Q_A:

$$CEF = \frac{Q_B}{Q_A} \tag{6.13}$$

6.3.1.2 Maximization of Anisotropy

Anisotropy measures the averaged anisotropy of the image with the help of pixel-wise directional entropy. The changes in the directional entropy are used to calculate anisotropy of an image and hence evaluate the image quality [131]. The Renyi entropy has been calculated to determine the local entropy of an image by associating a distribution for every pixel. The Renyi entropy in terms of discreet space-frequency distribution *P[n, k]*:

$$R_\alpha = \frac{1}{1-\alpha}\ log_2\ (\sum_n \sum_k P^\alpha[n,k]) \tag{6.14}$$

$where\ \ k$ and n are the frequency and spatial variables. The values of $\alpha \geq 2$ suggested for space-frequency distribution [159]. The special-frequency information of an image extracted using Pseudo-Wigner distribution (PWD) [202]. The discrete form of Wigner distribution [203] is given as follows: $W_z[n,k] = \sum_{m=-\frac{N}{2}}^{\frac{N}{2}-1} z[n+m]\ z^*[n-m]\, e^{-2i\left(\frac{2\pi m}{N}\right)k}$ (6.15)

$where\ n$ is discrete time variable, k is discrete frequency variable, m is a shifting parameter and $z[n]$ is a 1-D data sequence of an image with N number of pixels. The PWD normalized using quantum normalization as: $Q[n,k] = W[n,k]W^*[n,k]$, followed by $\check{P}_n = \frac{Q[n,k]}{\sum_k Q[n,k]}$,

where W^* is a complex conjugate of W. The normalization of PDW is known as probability distribution, $\check{P}_n$, which is used to compute Renyi entropy in following manner:

$$R_3[n] = \frac{1}{2} log_2\left(\sum_{k=1}^{N} \check{P}_n^3[k]\right) \quad (6.16)$$

The above equation helps to obtained entropy, $R_3[n, \theta_s]$ for every pixel of an image, where θ_s denotes S different orientations to calculate this entropy. The expected value of Equation (6.16) is obtained as follows:

$$\bar{R}[\theta_s] = \sum_n R_3[n, \theta_s]/M \quad (6.17)$$

where M denotes the size of the image. The expected value of entropy for an image measured using six predefined orientations ($0^\circ, 30^\circ, 60^\circ, 90^\circ, 120^\circ, 150^\circ$). The variance of these expected values is known as the anisotropy of the image.

$$\sigma(t) = \sqrt{\sum_{s=1}^{S} (\mu - \bar{R}\ (\theta_s))^2/S} \quad (6.18)$$

where μ is the mean value of $\bar{R}[t, \theta_s]$. The anisotropy of an image differentiates the presence of noise, where image having more noise resulting smaller anisotropy.

6.4 Material and Methods

The present study was a 'prospective observational cohort study' performed using data gathered during routine clinical work up of patients, after due written informed consent from the patients or his/her legal guardian. No additional sequences were performed for the purpose of data analysis alone while the images were used for post-processing using multi-stable DSR after de-identification of patient identity at the level of imaging unit itself. This ensured strict confidentiality and that no chances of patient identity being transferred outside the purview of the clinical management team. The study was conducted over a duration of

two years, data constituted of images of patients referred for MRI, as a part of routine clinical protocol during the course of their evidence-based management.

6.4.1 Patients selection

Ten consecutive cases where a clinical suspicion of pituitary microadenoma was raised and in whom the MRI had a suspicion of a lesion were included for image evaluation and processing. These cases were diagnosed based on the established criteria [204-206], patients with other confounding factors like history of past or active cranio-spinal infection, systemic illness and any ongoing chronic illness, were however excluded. Patients having other morphologically demonstrable abnormality on routine MRI sequences were also excluded.

6.4.2 Imaging

MR Imaging was performed on a 1.5 Tesla system, equipped with an actively shielded whole body magnet (Magnetom Avanto, Siemens medical system, Erlanger, Germany) with latest software platform (Syngo Version BV-I7A). The imaging has been performed using a quadrature bird-cage transmit receive coil (8 channel). A pre-standardized protocol was followed for routine morphological imaging. This included high resolution anatomical images acquired with a T1-weighted sagittal 3D MPRAGE sequence (TR 7.1, TE 3.45ms, TI 1000 ms, and flip angle 7 degrees, FOV 256mmx256mm and slab thickness 150mm) for fusion of the dynamic contrast enhanced (DCE) imaging data, along with T2, FLAIR sequences as provided by the vendor propriety software. The acquisition matrix was 256x192x128, reconstructed voxel resolution of 1.0mm x 1.0mm x 1.33mm. The DCE MRI was performed using three-dimensional Fourier transformed T1W TSE (turbo spin echo) sequence (TR/TE/FOV= 540 msec/13 msec/25 cm) with pre-programmed multi-acquisition mode (seven acquisitions) over a period of 2 minutes and 34 seconds. The sequence

consisted of seven sections in coronal plane from the anterior clinoid (AC) process to the dorsum sellae (DS). The slices were placed at a distance factor of zero and were angulated to be laid perpendicular to the AC-DS line to minimize the volume averaging artifact from the dorsum sellae and clivus. Each acquisition during the DCE was about 15 seconds in duration with the first acquisition being a pre-contrast mask (reference) image. Subsequent images were acquired during active contrast injection using a dual head pressure injector through an 18 gauge intravenous cannula placed in an arm vein. A dose of 0.05 mmol/kg body weight of gadolinium was injected intravenously followed by a saline bolus chase of 20 ml.

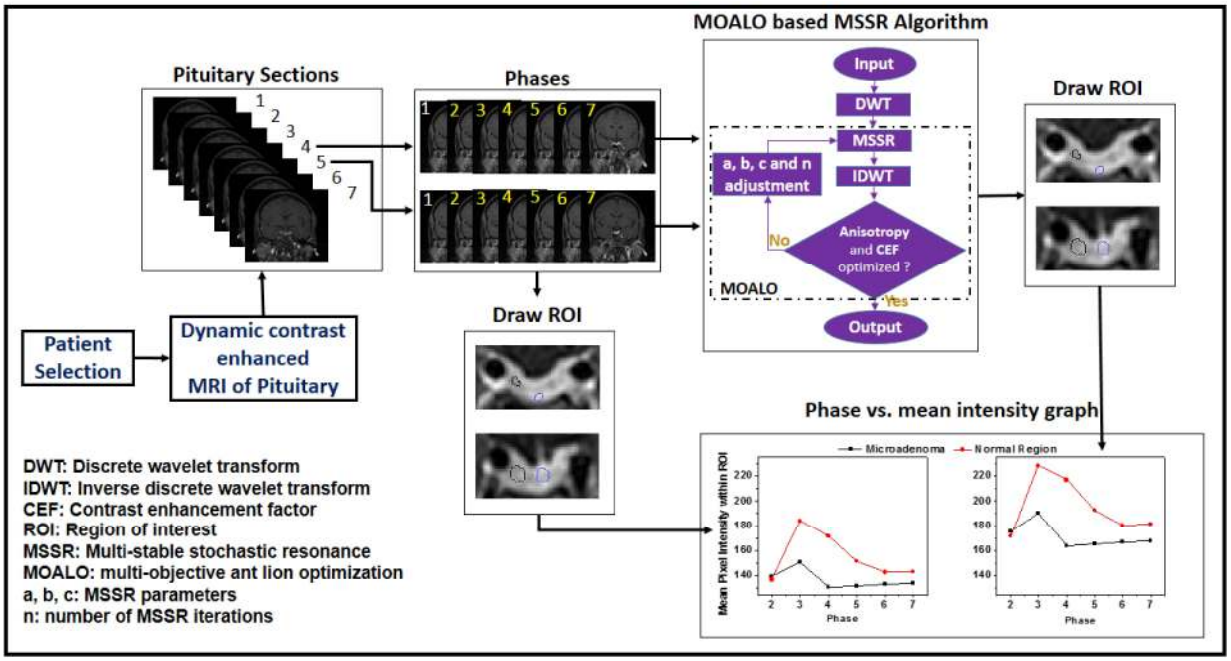

Figure 6-2: Overview of material and methods for proposed algorithm

6.4.3 Image Analysis & Evaluation

Initially on call, junior radiologists analyze and report the routine images followed by repeat examination and validation by a senior radiologist (A.V). The DCE data was however, prima-facie evaluated by the senior radiologist and reported prior to viewing the routine MR imaging, to exclude any kind of observer bias for the presence or absence of microadenoma.

Secondly, the off line workstation (Siemens medical system, Erlangen, Germany) helps in quantitative evaluation of the screen pixel intensity normalized over time scale at each spatial position was done by drawing circular region of interest (R.O.I) over to pre-identify areas of delayed enhancement. This was based on the observation that the infundibulum (pituitary stalk) enhances first followed by the gland parenchyma and then a centrifugal opacification of the anterior lobe over a period of 30-60 seconds [207]. The pathological tissue within the gland however remain as non-enhancing areas in these early phases and show contrast pooling later on [205]. Curves were generated to evaluate the discrepancy in phase at which peak gland and adenoma enhancement occurs as well as the magnitude of enhancement in each of these structures.

6.4.4 Image selection and application of multi-stable DSR

As discussed, radiologists analyze the DCE data for the confirmation of microadenoma using the automated mean intensity curves on the off line workstation (Siemens Medical system, Erlangen, Germany). Previously, the similar curve has been drawn to find the correlation between basal and stimulated conditions [208]. The present study also computed the mean intensity vs. phase curves for normal and microadenoma regions and obtained the increased gap between these two curves, which increased the confidence level of diagnosis. The algorithm enhanced the images using MOALO optimized MSSR. For this purpose, MSSR processed approximation coefficients of wavelet transform are given in Equation (6.6). These processed coefficients are reconstructed after taking the inverse DWT. The values of variables parameters (a, b, c) used in Equation (6.6) are derived with the help of MOALO for the maximization of objective functions expressed in Equations (6.13) and (6.18). Further, this formulation helps to produce the enhanced images, which are used to draw the mean

intensity vs. phase curve. It has been observed that fourth and fifth sections of pituitary gland keep maximum cross-sectional information in comparison to other sections. Hence, these two section images were used to draw the mean intensity curve. The post processing excluded the first phases of both sections as we assumed that the injected contrast might not reach to pituitary in the first phase.

Further, two manually prepared masks have been applied to create ROIs on pituitary gland for normal and microadenoma regions as shown in Fig. 6.3. The fourth section images have been undergone these masks and calculated the mean pixel intensity for each region. The same has been repeated for six phase images (second to seven phase images) belong to the fifth section as well. The average of fourth and fifth section images has been used to draw the mean intensity curves against different phases.

6.5 Results and Discussion

6.5.1 Image analysis using optimized MSSR

The MSSR can be implemented as three different SR models namely mono-stable, bi-stable and tri-stable models. Bi-stable and tri-stable models, where the Brownian particle can move between two and three wells respectively, on the other hand, this particle can rotate within a single well in mono-stable model and no resonance occurs, hence this study analyzes the bi-stable and tri-stable models. The parameters values for each model were optimally obtained for the maximization of CEF and anisotropy of image using MOALO. Both bi-stable and tri-stable models of MSSR were optimized individually and were compared for the dataset of simulated T1 and T2 weighted sequences of MRI available at BrainWeb (http://www.bic.mni.mcgill.ca/brainweb/). Further, this algorithm has been applied on real DCE MRI data and obtained promising results. The comparison study has also been carried

out between the classical quartic bi-stable SR and proposed MSSR techniques, where the quantitative analysis shows a clear edge of the proposed technique on the dataset images.

Figure 6.3 shows the analysis of bi-stable and tri-stable states of MSSR technique, where the input T1 and T2 weighted MRI data of brain are shown in the first column. The output images of bi-stable state shown in second column and the output images of tri-stable state shown in the third column. The output images of both states shows better differentiation of gray-white matter in comparison to the input images. The randomly selected region in yellow box has separately shown in enlarged view to analyze the tissue differentiation capability of both the models of MSSR technique. The images obtained in case of tri-stable state appears better in terms of gray-white matter differentiation than the bi-stable state. The quantitative evaluation of performance parameters in terms of CEF and peak signal to noise ratio (PSNR) indicates the clear advantage of tri-stable over the bistable state of MSSR. The tri-stable state is useful for contrast enhancement while keeping the high PSNR.

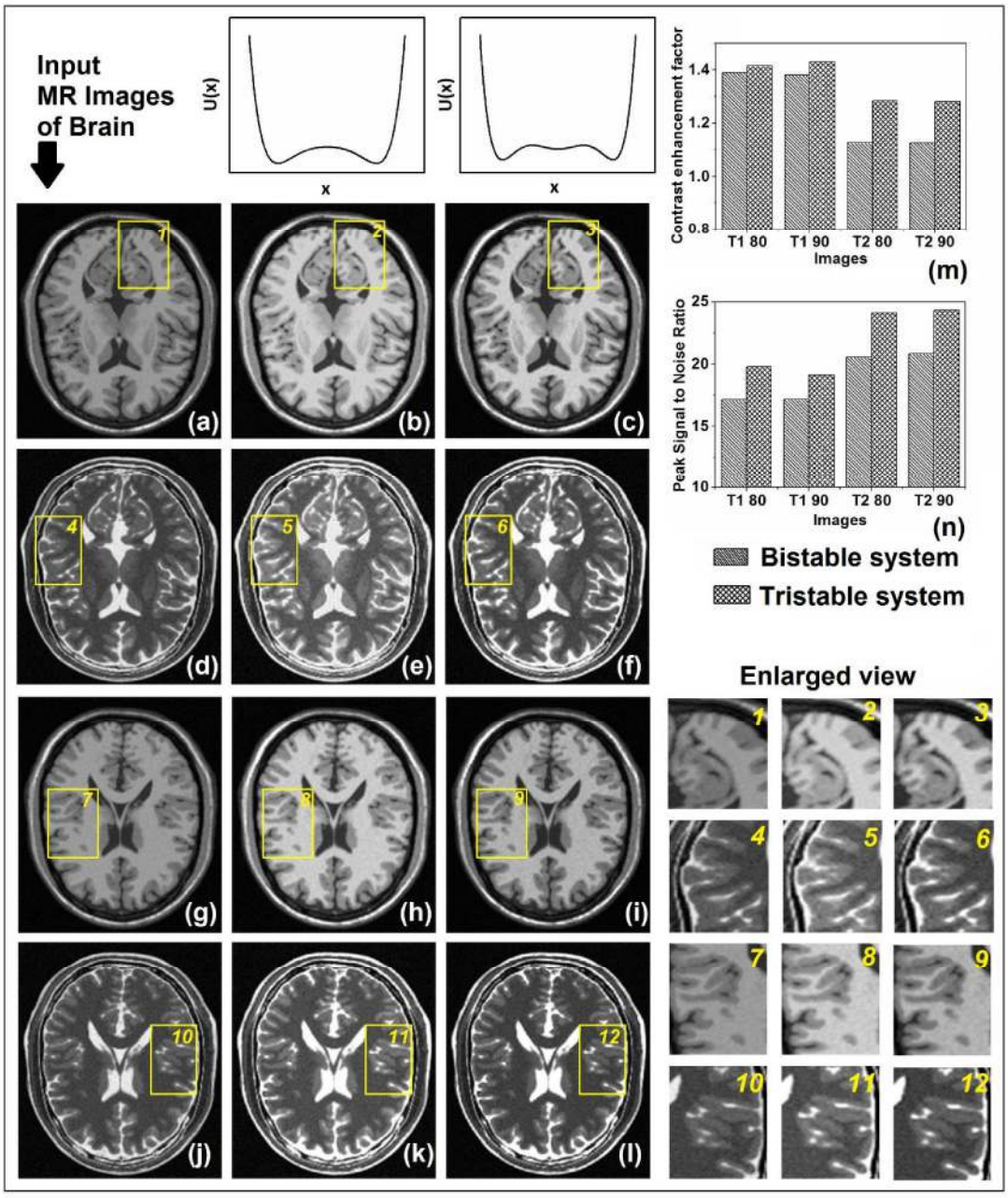

Figure 6-3: Qualitative and quantitative evaluation of proposed MOALO based MSSR algorithm on simulated T1, T2 weighted images of dataset, (a, g) input T1W image with 80th slice and 90th slice (T1 80 and T1 90), respective processed images in (b, h) bistable mode, (c, i) in tri-stable mode, (d, j) input T2W image with 80th slice and 90th slice (T2 80 and T2 90), respective processed images in (b, h) bistable mode, (c, i) in tri-stable mode, (m, n) comparison of CEF and PSNR of MSSR in bi-stable and tri-stable mode

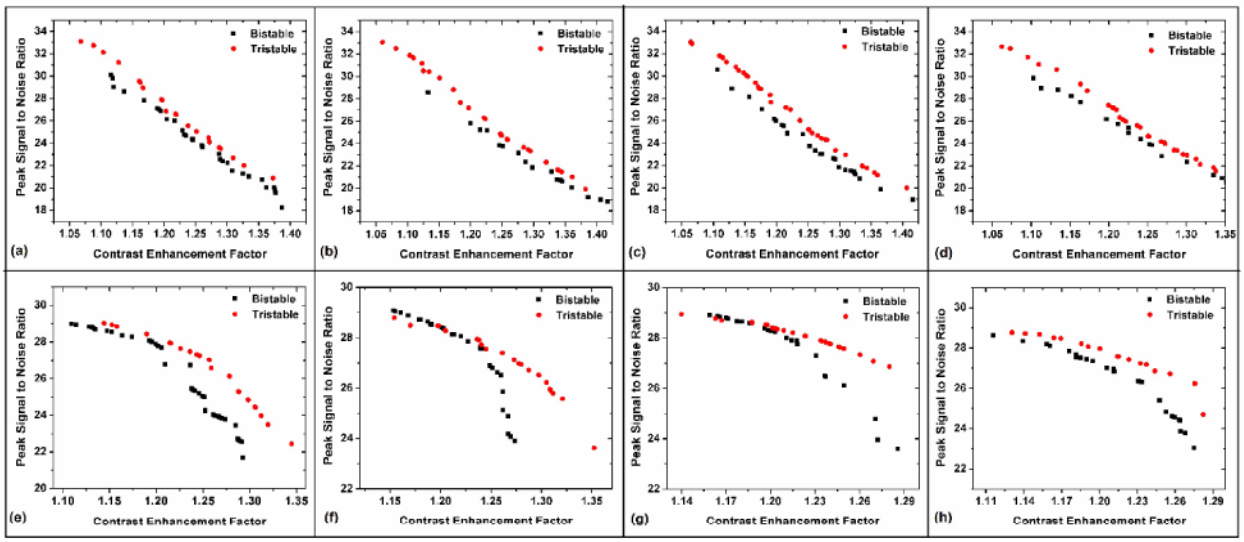

Figure 6-4: Pareto front surfaces of two objective functions PSNR and CEF for T1 60, T1 70, T1 90, T1 100, T2 60, T2 70, T2 90 and T2 110 simulated MR images

The pareto front surfaces shown in Fig. 6.4 demonstrate the relation between CEF and PSNR of T1-weighted and T2-weighted images obtained from BrainWeb dataset. Each discrete point in the plots has been obtained for a specific set of DSR parameters using MOALO algorithm. The discreet points belong to tri-stable state (points in red) lays above to points belong to bistable state (points in black), which indicates that the bi-stable state has low PSNR for approximately equal CEF value of both states. At the same time, bi-stable state has low CEF for approximately equal PSNR value of both states. This analysis also shows that there are noteworthy advantages of tri-stable over the bi-stable state.

6.5.2 MSSR for the detection of adenomas in pituitary gland

The present algorithm is implemented on DCE MRI data for improved detection of microadenoma. The radiologists examine the microadenomas by observing the pattern of enhanced and non-enhanced regions of pituitary gland in different phases. The proposed algorithm scales up the gray level to a greater extent in enhanced region in comparison to other regions of the pituitary gland, which helps to produce better contrast between the

tissues belongs to microadenoma and normal region. The same is also helpful in the quantitative analysis, as it enables to draw the accurate ROIs, which is further used to plot the mean intensity curve. Figure 6.5 shows the qualitative analysis of the MRI data for Test 1. The first row of Fig. 6.5 shows all seven sections of pituitary in the coronal plane obtained from MRI scanner and works as the inputs to the proposed algorithm. The images shown in second row are the cropped enlarged regions corresponding to first row images. It can be noted that the pituitary is well seen in fourth (Fig. 6.5 (d)) and fifth sections (Fig. 6.5 (e)), hence for better analysis, only these two sections used to plot the mean intensity curve. The third row of the figure shows the MOALO based MSSR enhanced images corresponding to first row images. The images shown in fourth row are cropped enlarged regions corresponding to third row images. These images shows better tissue contrast in comparison to corresponding second row images for all seven sections of pituitary gland. The fifth and seventh row images are the six phases (second to seventh phases) of fourth section images obtained from MRI scanner and MOALO based MSSR enhanced images respectively. The images shown in eighth row are cropped-enlarged pituitary have better contrast between the microadenoma and normal region in comparison to sixth row images. Figure 6.6 shows the input and processed images using proposed algorithm for case 2 suspicion of pituitary microadenoma.

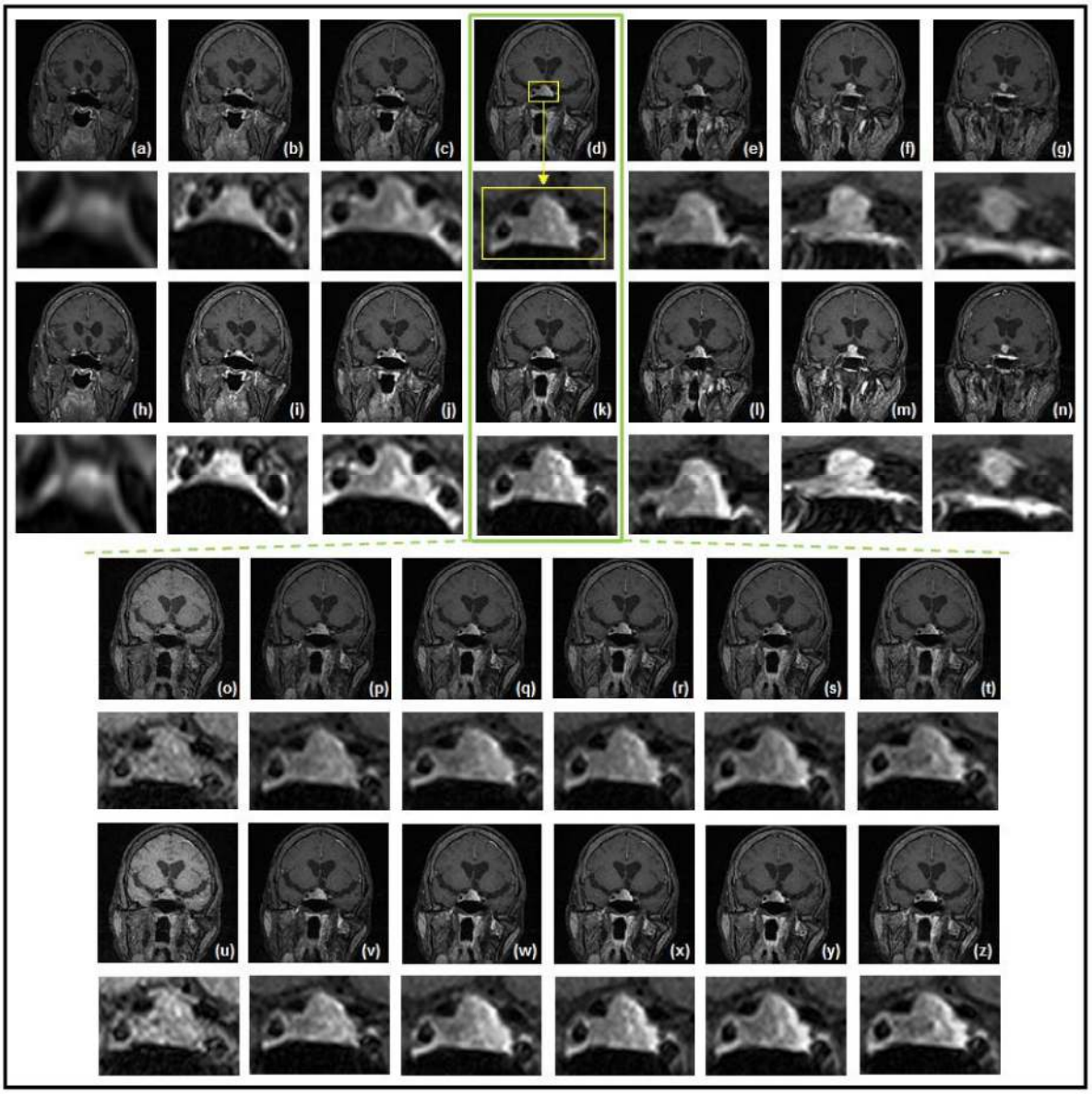

Figure 6-5: DCE MR images of case 1 suspicion of pituitary microadenoma, (a-g) all seven sections of coronal planes from the anterior clinoid to the dorsum sellae, the enlarged view of pituitary gland are shown in below to respective images, (h-n) processed images using proposed MOALO based MSSR algorithm respective to images shown in (a-g), (o-t) six phases (second to seventh phase) of plane 4, (u-z) processed images using proposed MOALO based MSSR algorithm respective to images shown in (o-t)

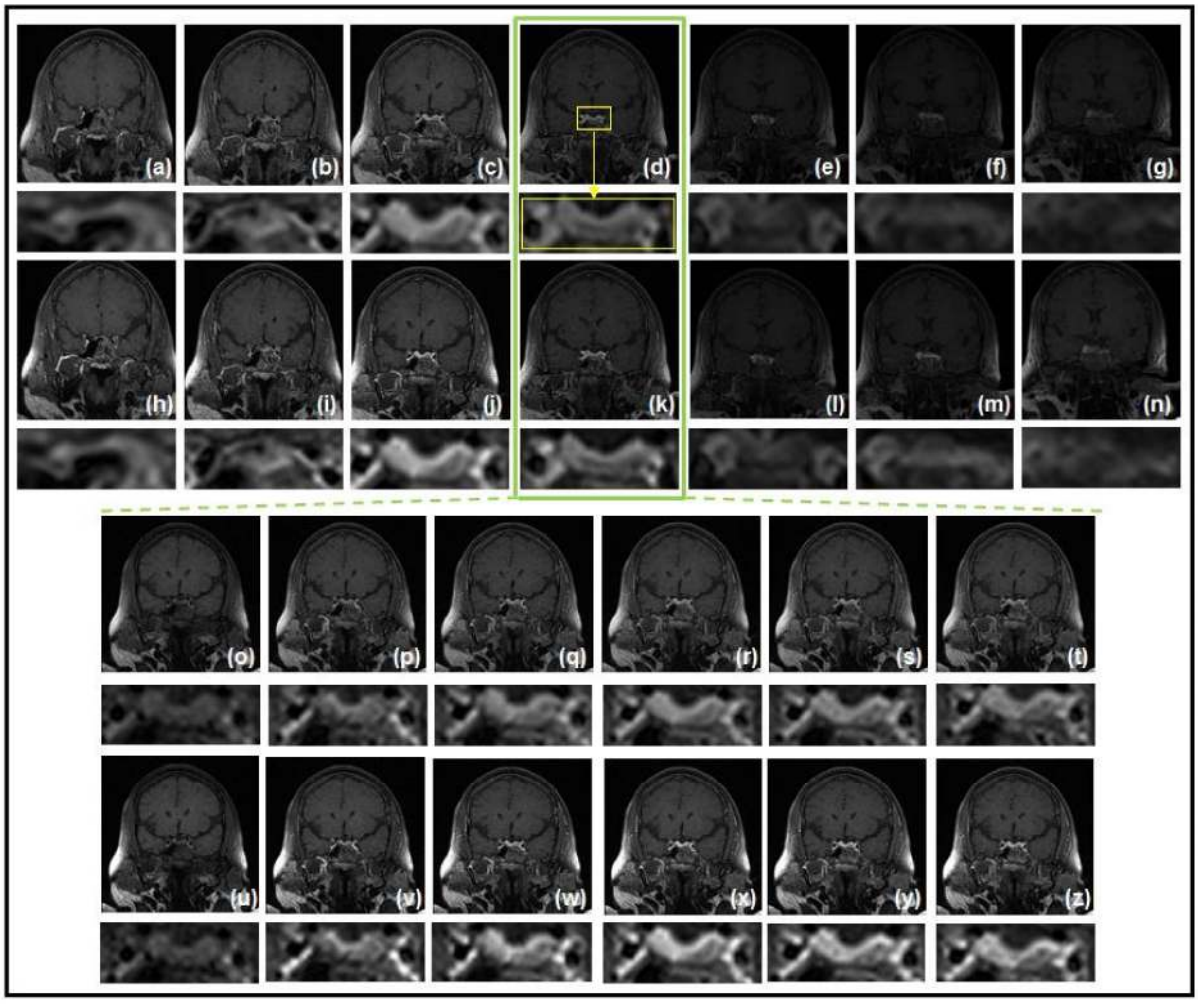

Figure 6-6: DCE MR images of case 2 suspicion of pituitary microadenoma, (a-g) all seven sections of coronal planes from the anterior clinoid to the dorsum sellae, the enlarged view of pituitary gland are shown in below to respective images, (h-n) processed images using proposed MOALO based MSSR algorithm respective to images shown in (a-g), (o-t) six phases (second to seventh phase) of plane 4, (u-z) processed images using proposed MOALO based MSSR algorithm respective to images shown in (o-t)

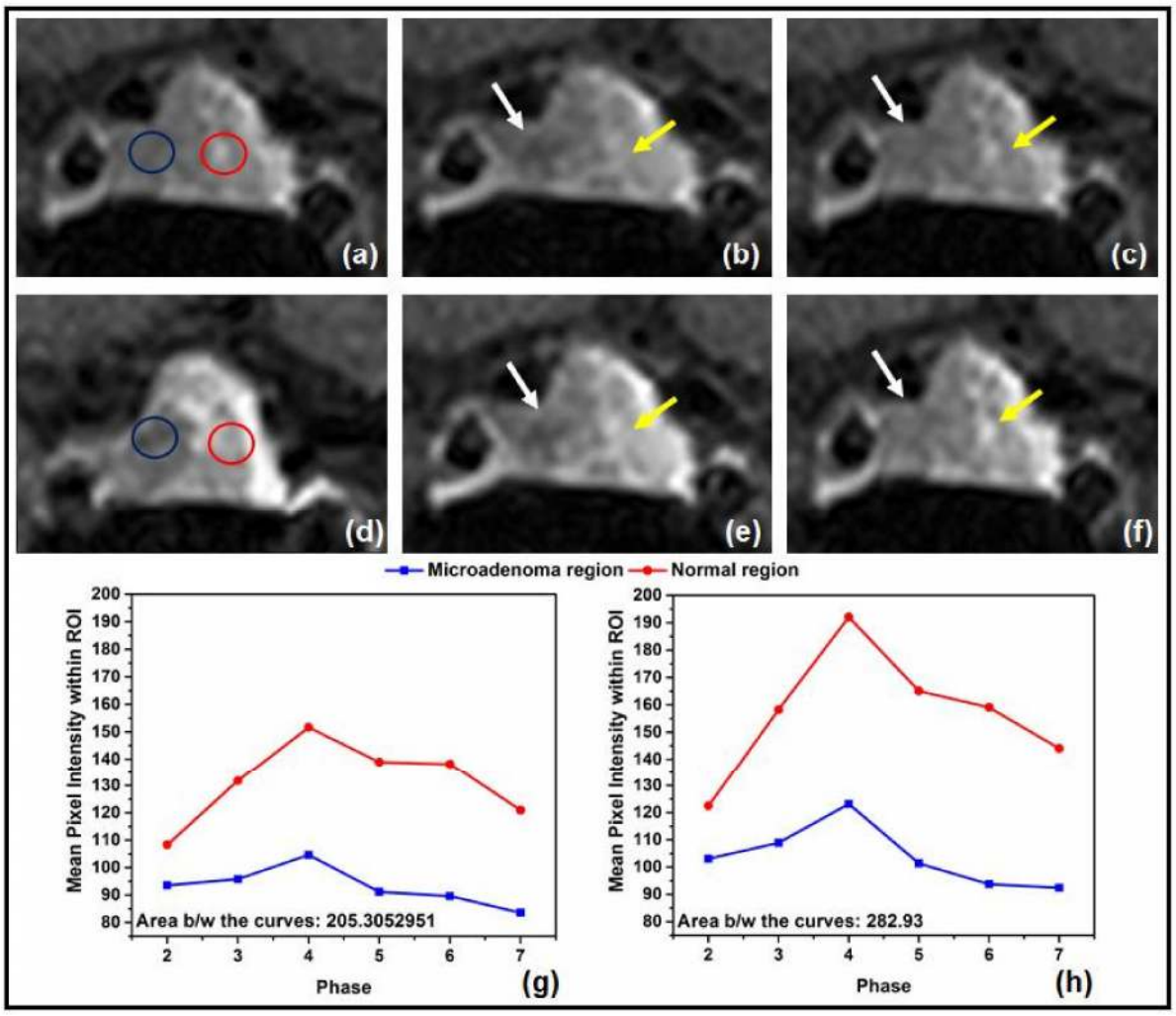

Figure 6-7: Case 1 suspicion of pituitary microadenoma (a, d) enlarged pituitary of algorithm processed images showing placement of ROIs for microadenoma (blue circle) and normal region (red circle), (b, c) cropped input, (e, f) cropped output fourth and fifth phases of section 4, (g) mean intensity curves for original input DCE MR images and (h) obtained by proposed algorithm for section 4 and section 5.

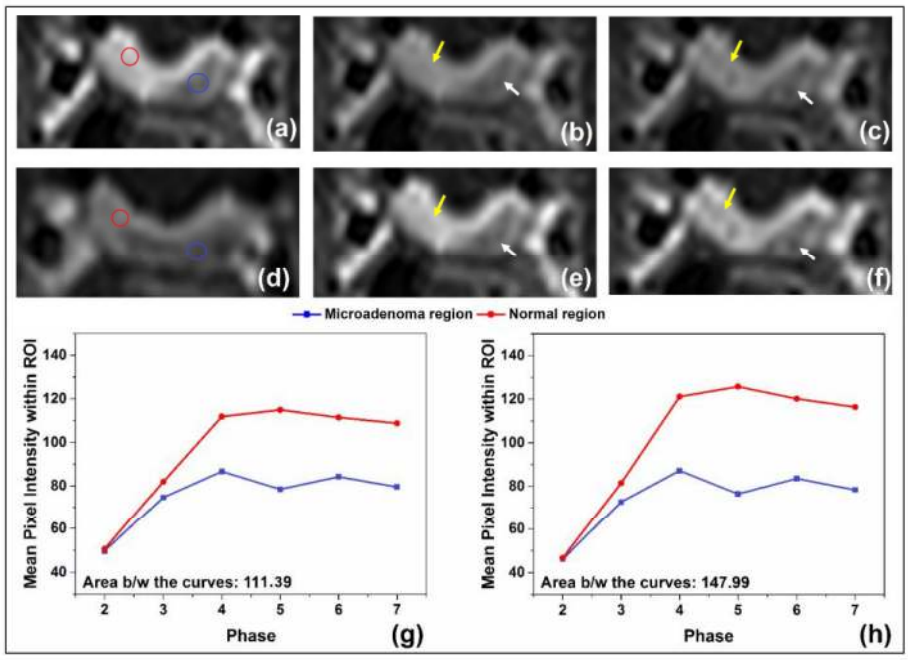

Figure 6-8: Case 2 suspicion of pituitary microadenoma (a, d) enlarged pituitary of algorithm processed images showing placement of ROIs for microadenoma (blue circle) and normal region (red circle), (b, c) cropped input, (e, f) cropped output fourth and fifth phases of section 4, (g) mean intensity curves for original input DCE MR images and (h) obtained by proposed algorithm for section 4 and section 5

Figure 6.7 shows dynamic contrast enhanced T1 weighted TSE images (fourth and fifth phases) in oblique coronal plane through the center of sella tursica before (Fig. 6.7 (b, c)) and after (Fig. 6.7 (e, f)) the application of proposed MOALO based MSSR algorithm. Note the quadrangular geographic shaped microadenoma (white arrow on the right side) seen in the two consecutive sections shows less enhancement as compared to the normal pituitary gland (yellow arrow on the left side). Notable is the visible difference in contrast of images with the post-MOALO based MSSR images which makes manual ROI placements more accurate and confident (as seen in Fig. 6.8 (a)). This subjective observation is validated on the dynamic curves where the Y-axis interval between the pre & post MOALO based MSSR curves shows a definite numerical increase. Though the time to peak in terms of phases remains the same, the magnitude of peak value shows an increase in the mean intensity

value. The greater difference between the curves obtained using proposed MOALO based MSSR algorithm means that it improves the tissue contrast between the microadenoma and surrounding healthy tissues, which strongly confirms the microadenoma in the pituitary. Figure 6.8 shows placement of ROIs on section 4 and section 5 (Fig. 6.8 (a, d)) and the plots obtained using their six phases (Fig. 6.8 (g, h)) for case 2.

6.5.3 Comparison between Multi-stable and classical DSR

This work also compares the multi-stable and classical quartic bi-stable SR model [136] on standard BrainWeb dataset images. For this purpose, both the models used optimized DSR parameters obtained from MOALO algorithm for the enhancement test T1 and T2 weighted image. The value of multi-stable model parameter 'c' has no constraint to choose only positive or negative values, which means multi-stable model can behave either as bi-stable or tri-stable model. The constraints on number of iteration 'n' kept same to observe the true competition between both the models. The results shown in terms of Pareto front surfaces plotted between PSNR and CEF as shown in Fig. 6.9. The multi-stable model shows higher trade-off values for T1 weighted sequences in comparison to classical quartic bistable SR model. In case of T2 weighted sequences, the classical SR model perform better in terms of PSNR at very low CEF, however these values produces insufficient contrast. The input images shown in Fig. 6.10 are T1 60 and T2 70, the processed images obtained corresponding to maximum CEF point on Pareto front surface for classical quartic bistable model, rather for any near optimal parameter(s). The image obtained for multi-stable model is corresponding to point horizontally forward on multi-stable curve. The MSSR method enhances the T1 and T2 weighted images to the greater extend in comparison to classical SR model.

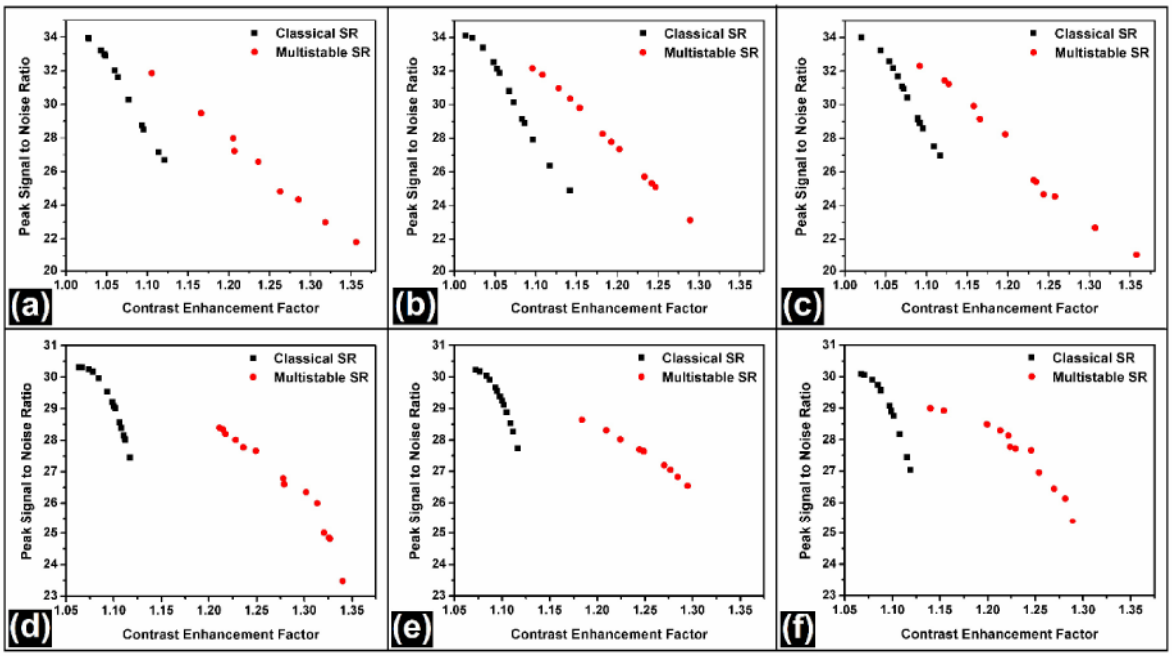

Figure 6-9: Comparison between classical SR and MSSR technique using pareto front surfaces of two objective functions PSNR and CEF for T1 60, T1 70, T1 80, T2 70, T2 80 and T2 90 simulated MR images

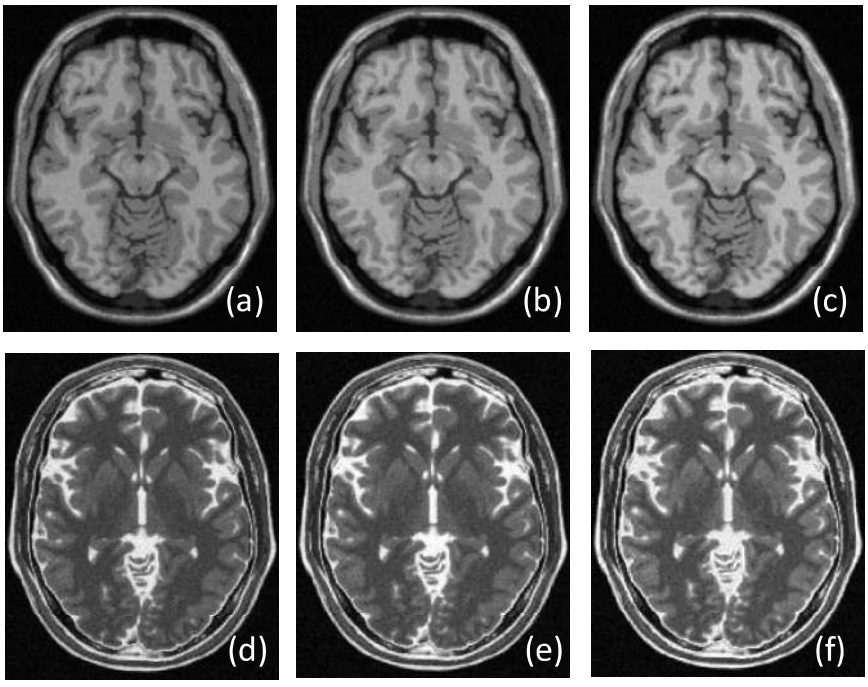

Figure 6-10: (a, d) Input T1 and T2 weighted simulated MR images, (b, e) MOALO based classical quartic bistable processed images, (c, f) MOALO based MSSR processed images respective to first column images

6.5.4 Comparative study of MOALO with other optimization algorithms

This section evaluate the effectiveness of MOALO algorithm against multi-objective NSGA-II [90], Bat [97], PSO [94] on total ten T1 and T2 BrainWeb dataset images. The performance measures of optimization algorithm are based on convergence to benchmark set, which corresponds to (i) normalized generational distance (GDn) [209], diversity of the solutions, which corresponds to (ii) spacing and (iii) max spread [210]. Table 6-1 shows mean and standard deviation (SD) of these measures for NSGA II, BAT, PSO and ALO algorithms. Lower value of GDn indicates the better convergence of solution, whereas lower value of spacing and higher value of maximum spread indicates that the solution has better diversity. The benchmark Pareto front has been derived from best solution obtained by running each optimization algorithm five times, while keeping sixty iterations. This benchmark Pareto front has been compared with Pareto fronts of considered optimization algorithms for comparison as shown in Fig. 6.11. All Pareto fronts have been normalized to measure their performance. In this study, Pareto fronts obtained for each optimization algorithm while considering twenty iterations. As results shown in Table 6-1, ALO performs better in terms of convergence and diversity measures for T2 weighted dataset images. Bat optimization produced better convergence for T1 weighted dataset images just followed by ALO. However, Bat performs poor at the end of diversity, at the same time ALO performs best among considered optimization algorithms.

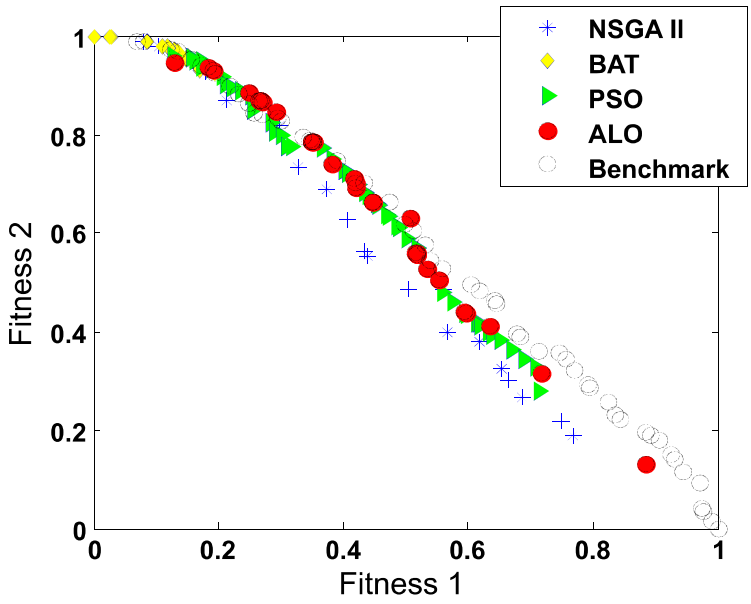

Figure 6-11: Normalized Pareto fronts for the maximization of objectives (Fitness 1: CEF, Fitness 2: PSNR) on 60th slice of T1 weighted image obtained from BrainWeb

Table 6-1: Performance comparison of different multi-objective optimization methods on ten simulated MRI dataset images

Method	Dataset	GDn		Spacing		Max Spread	
		mean	SD	mean	SD	mean	SD
NSGA II	T1	0.042	0.015	0.091	0.027	1.079	0.213
	T2	0.043	0.030	0.081	0.032	0.875	0.335
BAT	T1	**0.015**	0.004	0.047	0.017	0.217	0.035
	T2	0.078	0.039	0.044	0.012	0.523	0.319
PSO	T1	0.029	0.004	0.018	0.006	0.881	0.115
	T2	0.046	0.024	0.026	0.006	0.748	0.218
ALO	T1	0.025	0.007	**0.015**	0.005	**1.258**	0.086
	T2	**0.039**	0.027	**0.014**	0.005	**0.986**	0.179

The present study has implemented the two complementary image quality measures: CEF and PSNR to achieve their maximization. Further, the quality of image is subjective matter and may depends on parameters such as: contrast, signal to noise ratio, sharpness and

dynamic range. The better performance may be achieved by adding more image quality measure(s) as the objective function. Further, it can be stated that present algorithm is an optimization-based enhancement technique, hence, the number of iteration should be carefully chosen on the basis of complexity of the problem, otherwise optimization may stuck in pre-mature settlement and yield sub-optimal results.

6.6 Conclusions

In the present chapter MSSR – MOALO based hybridized algorithm has been proposed for optimum enhancement of MRI data. The hybridization of MSSR with MOALO algorithm facilitated the optimal selection of parameter associated with the dynamics of MSSR using the trade-off between the CEF and PSNR. The proposed algorithm was tested on simulated and real MRI data. The performance of MSSR evaluated on simulated MRI data for its bi-stable and tri-stable state operations, where tri-stable state has shown better results. The algorithm was then applied to real MRI dataset for the analysis of lesion cases of pituitary gland (selected as ROI), the output results obtained in terms of enhancement achieved for ROI and mean intensity based dynamic curves were helpful in diagnosis of microadenoma with increased level of confidence. The proposed algorithm has been performing better in comparison to quartic bi-stable based DSR, CLAHE, BPDFHE, LMMSE+CLAHE and LMMSE+BPDFHE based enhancement algorithms on the BrainWeb dataset of simulated MRI data. The effectiveness of MOALO algorithm has been evaluated with the help of quantitative comparison against NSGA II, BAT, and PSO in terms of convergence and diversity of solutions. The MOALO algorithm shows best mean values of GDn as 0.032, Spacing as 0.014 and Max Spread as 1.122 on dataset of ten images.